Analysis of Serial Engagement and Peptide-MHC Transport in T Cell Receptor Microclusters

Omer Dushek and Daniel Coombs
Department of Mathematics and Institute of Applied Mathematics, University of British Columbia, Vancouver, Canada

ABSTRACT In experiments where T cells interact with antigen-presenting-cells or supported bilayers bearing specific peptide-major-histocompatibility-complex (pMHC) molecules, T cell receptors (TCR) have been shown to form stable micrometer-scale clusters that travel from the periphery to the center of the contact region. pMHC molecules bind TCR on the opposing surface but the pMHC-TCR bond is weak and therefore pMHC can be expected to serially bind and unbind from TCR within the contact region. Using a novel mathematical analysis, we examine serial engagement of mobile clustered TCR by a single pMHC molecule. We determine the time a pMHC can be expected to remain within a TCR cluster. This also allows us to estimate the number of clustered TCR that are serially bound, and the distance a pMHC is transported by the clustered TCR. We find that TCR-pMHC binding alone does not allow substantial serial engagement of TCR and that the pMHC molecules are usually not transported to the center of the contact region by a single TCR cluster. We show that the presence of TCR coreceptors such as CD4 and CD8, or pMHC dimerization on the antigen-presenting cells, can substantially increase serial engagement and directed transport of pMHC. Finally, we analyze the effects of multiple TCR microclusters, showing that the size of individual clusters only weakly affects our prediction of TCR serial engagement by pMHC. Throughout, we draw parameter estimates from published data.

INTRODUCTION

T cells play a central role in adaptive immunity by regulating immune responses and performing targeted killing of infected cells. For T cells to carry out these functions they must be stimulated by antigen-presenting cells (APC) bearing cognate antigen. Stimulation is mediated by interactions between T cell receptors (TCR) and specific antigen presented in the form of peptide-major-histocompatibility complexes (pMHC), in a tight adhesion region between the T cell and APC (1,2). In this region, known as the immunological synapse (IS), fewer than 10 agonist pMHC molecules have been shown to transduce sufficient intracellular signaling to cause measurable stimulation of T cells (3–5). Further, the TCR-pMHC bond is weak, with solution K_D usually in the μM range (6).

A partial explanation of the sensitivity of T cells to such weak stimuli was proposed by Valitutti et al. (7). TCR downregulation was measured over the course of several hours of T cell interaction with APC carrying a known number of antigenic pMHC. The ratio of downregulated TCR to number of pMHC was found to be as high as 200. Assuming that every internalized TCR has previously bound pMHC, this suggests that pMHC sequentially bind hundreds of TCR in the IS. This is known as the serial-engagement hypothesis. Similar results were found by Itoh et al. (8) but the notion of serial engagement was weakened by findings that TCR that have never bound pMHC can be internalized in a pMHC-dependent manner (9). Further investigation revealed that when few pMHC are present on the APC, TCR are downregulated so rapidly that a strict serial engagement model could not fit the data (10,11). Rather, a model allowing for downregulation of nearby, unstimulated TCR, in a TCR-density-dependent manner, provided a more plausible explanation (11). The importance of serial engagement of TCR for T cell activation has been further challenged by data of Holler and Kranz (12), which did not show a decline in T cell activation by high-affinity pMHC. We reanalyze parts of this data here.

We see that the rate of engagements (i.e., the hitting rate) between TCR and pMHC is of great importance. Using a simple mathematical model, Wofsy et al. (13) calculated the hitting rate for a single pMHC moving diffusively on the APC surface. Using measured parameters for the TCR-pMHC bond, it was found, for instance, that a single agonist pMHC can engage 5–35 TCR during one sojourn in the IS. The highest rates of serial engagement were achieved by those pMHC that bind TCR very transiently. On the other hand, fast-dissociating pMHC would lead to only weak signaling of individual TCR. These considerations led to a model of overall pMHC signaling efficacy based on the lifetime of the TCR-pMHC bond, where the optimal pMHC has a lifetime that is high enough for reliable signaling of individual TCR, but low enough for serial engagement to proceed efficiently (7,14,15). These verbal predictions were confirmed experimentally and theoretically in a series of experimental and theoretical articles (16–18).

In the calculations of Wofsy et al. (13), it was assumed that TCR are distributed homogeneously within the IS. It has since been shown that TCR aggregate into half-micron-sized clusters, often referred to as TCR microclusters, in T cell synapses formed with both APC (19) and suspended planar bilayers (19–21) bearing agonist pMHC. These TCR clusters form in the periphery of the IS, a region known as the peripheral supramolecular activation cluster (pSMAC), and

Submitted July 5, 2007, and accepted for publication December 31, 2007.

Address reprint requests to Daniel Coombs, E-mail: coombs@math.ubc.ca.

Editor: Byron Goldstein.

0006-3495/08/05/3447/14 $2.00

doi: 10.1529/biophysj.107.116897

migrate toward the center of the IS (the central-SMAC (cSMAC)) (19). Various molecules in the signaling cascade that begins with a pMHC interacting with a TCR have been shown to localize in pSMAC clusters and not in the cSMAC (19,20). TCR clusters are observed to form when bilayer pMHC densities are as low as 0.2 μm^{-2} (21).

Weak TCR-pMHC interactions can also be stabilized by more complex binding reactions. For instance, the cell-surface coreceptors CD4 and CD8 (22) are thought to bind the nonpolymorphic regions of the pMHC molecule (23), strengthening the TCR-pMHC interaction. The cytoplasmic tails of CD8 and CD4 are also associated with Lck, a molecule known to interact with the cytoplasmic tail of engaged TCR, perhaps further stabilizing the complex (24). In a similar vein, pMHC are thought to form multimeric complexes that may allow for stabilization of bonds formed by the individual pMHC (further discussion below).

In this article, we revisit the calculations of Wofsy et al. (13) in the context of moving TCR clusters and stabilization of the TCR-pMHC bond by coreceptors and pMHC dimerization. We show that serial engagement, in the context of mobile clusters, is negligible unless the bond is stabilized, in which case substantial serial engagement of TCR by a single pMHC molecule will occur. We also show that stabilization is necessary for pMHC transport to the cSMAC within a single cluster and that pMHC transport to the cSMAC is well correlated with T cell stimulation. Finally, we consider a field of immobile clusters, and examine how many TCR a pMHC can expect to engage during one sojourn in the IS in such a situation.

MATHEMATICAL MODEL

We derive a model for the escape time of a pMHC molecule diffusing within the immunological synapse and potentially binding and unbinding from TCR. We do not resolve individual TCR in this model, nor do we consider TCR signaling after pMHC engagement of TCR. Principally, we are concerned with understanding how physical parameters of the TCR-pMHC interaction are related to pMHC motion within the IS and serial engagement of TCR by pMHC. TCR signaling and more complex effects within this model could be addressed using an agent-based approach (25).

Four-state escape time formulation from a mobile TCR cluster

We want to calculate the length of time that a pMHC is expected to remain within a TCR cluster before escaping. We model a particle (i.e., a pMHC molecule) advecting and diffusing in a two-dimensional membrane. The particle transitions between four states (i = A, B, C, and D) by a Markov process with first-order reactions between the states, as shown in Fig. 1. We define the escape time from some domain, for a particle in state i at position (x, y), to be $t_i(x, y)$.

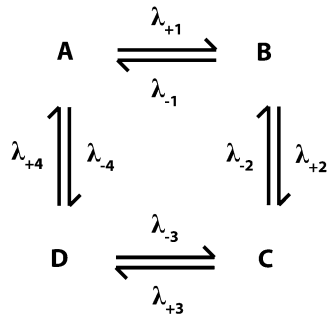

FIGURE 1 The most general reaction scheme we consider. Transitions between the four states occur with first-order reactions, with transition rates given by $\lambda_{\pm i}$. Detailed balance (microscopic reversibility) requires that $\lambda_1\lambda_2\lambda_3\lambda_4 = \lambda_{-1}\lambda_{-2}\lambda_{-3}\lambda_{-4}$. Specific reaction schemes are illustrated in Fig. 2.

This is calculated for a diffusing particle (without reactions) by solving the Poisson equation on the region of interest using Dirichlet (zero) boundary conditions (see Appendix A of Goldstein et al. (26) for a heuristic derivation based on a two-dimensional random walk). Following the procedure in the literature (13,26), we derive a system of equations governing the $t_i(x, y)$:

$$\begin{aligned}
D_A\nabla^2 t_A - \vec{V}_A\cdot\nabla t_A + \lambda_{+1}(t_B - t_A) + \lambda_{-4}(t_D - t_A) &= -1\\
D_B\nabla^2 t_B - \vec{V}_B\cdot\nabla t_B + \lambda_{+2}(t_C - t_B) + \lambda_{-1}(t_A - t_B) &= -1\\
D_C\nabla^2 t_C - \vec{V}_C\cdot\nabla t_C + \lambda_{+3}(t_D - t_C) + \lambda_{-2}(t_B - t_C) &= -1\\
D_D\nabla^2 t_D - \vec{V}_D\cdot\nabla t_D + \lambda_{+4}(t_A - t_D) + \lambda_{-3}(t_C - t_D) &= -1.
\end{aligned} \tag{1}$$

D_i values are the diffusion coefficients of the particle in each state, $\vec{V}_i$ values are the advection velocity vectors, λ_i values are the transition rates, and we set $t_i = 0$ on the domain boundary.

Although we will apply the general reaction scheme illustrated in Fig. 1 to several scenarios, we will always identify state $i = A$ with a free pMHC on the APC or supported planar bilayer and states $i = B, C, D$ with pMHC bound to molecule(s) on the T cell (e.g., TCR, CD4, CD8). Since the pMHC molecule undergoes directed motion toward the cSMAC only when bound to molecules within a cluster, we can make the equations simpler by working in the cluster reference frame (i.e., $\vec{V}_A = -\vec{V}$ and $\vec{V}_B = \vec{V}_C = \vec{V}_D = 0$), and picking the cluster velocity vector along a coordinate axis $\vec{V} = (V, 0)$. We further assume that, when bound, the pMHC has a negligible rate of diffusion (i.e., $D_B = D_C = D_D = 0$), to find

$$\begin{aligned}
D_P\nabla^2 t_A + V\partial t_A/\partial x + \lambda_{+1}(t_B - t_A) + \lambda_{-4}(t_D - t_A) &= -1\\
\lambda_{+2}(t_C - t_B) + \lambda_{-1}(t_A - t_B) &= -1\\
\lambda_{+3}(t_D - t_C) + \lambda_{-2}(t_B - t_C) &= -1\\
\lambda_{+4}(t_A - t_D) + \lambda_{-3}(t_C - t_D) &= -1,
\end{aligned} \tag{2}$$

where we set $D_A = D_P$, the free pMHC diffusion coefficient. We use the last three equations to solve for t_B and t_D in terms of t_A and so obtain a single equation for t_A:

$$D_P \nabla^2 t_A + V\frac{\partial t_A}{\partial x} = -\beta. \tag{3}$$

$\beta = 1 + \Lambda_1 + \Lambda_1\Lambda_2 + \Lambda_1\Lambda_2\Lambda_3$, where $\Lambda_i = \lambda_i/\lambda_{-i}$ are the transition affinities. We eliminated Λ_4 from β using the principle of detailed balance (microscopic reversibility) which requires that $\Lambda_1\Lambda_2\Lambda_3\Lambda_4 = 1$. For simplicity we will assume that the cluster is a square of side b.

We formulate the solution to Eq. 3 as $t_A(x, y) = \beta\,\Phi(x, y)$, with

$$\Phi(x,y) = \sum_{n=1}^{\infty} q_n(x)\sin\left(\frac{n\pi y}{b}\right). \tag{4}$$

After substituting in, we obtain

$$q_n(x) = \frac{2b^2((-1)^n - 1)}{D_P(n\pi)^3}\left[\exp\left(\frac{-x(V + w_n)}{2D_P}\right) - 1 + \exp\left(\frac{V(b-x)}{2D_P}\right)\left(1 - \exp\left(\frac{-b(V + w_n)}{2D_P}\right)\right) \times \sinh\left(\frac{x w_n}{2D_P}\right)/\sinh\left(\frac{b w_n}{2D_P}\right)\right], \tag{5}$$

where $w_n = \sqrt{V^2 + 4D_P^2(n\pi/b)^2}$. We note that the escape time is only dependent on transition affinities, through the parameter β, and not on the individual forward and backward reaction rates. We obtain the mean escape time by averaging over all possible starting positions of the pMHC,

$$\langle t\rangle = \beta\langle\Phi(x, y; V, D_P, b)\rangle = \frac{\beta}{b^2}\int_0^b\int_0^b \Phi(x, y; V, D_P, b)\,dx\,dy. \tag{6}$$

This averaging gives us a simple measure of the time a pMHC will spend in a single cluster, allowing us to easily understand the effects of changing the parameters of the TCR-pMHC interaction. Finally, the mean distance a pMHC molecule is transported by the cluster is then $\langle L\rangle = V\,\langle t\rangle$ where V is the cluster velocity.

Mean escape time and reaction rates determine the number of hits

We now derive expressions for the number of transitions between each state in Fig. 1 during a sojourn in a TCR cluster. We begin by calculating the probability, P_i, of finding the particle in state i by considering the transition matrix associated with Fig. 1 augmented by the conservation equation $P_A + P_B + P_C + P_D = 1$,

$$\begin{pmatrix} -\lambda_1 - \lambda_{-4} & \lambda_{-1} & 0 & \lambda_4 \\ \lambda_1 & -\lambda_2 - \lambda_{-1} & \lambda_{-2} & 0 \\ 0 & \lambda_2 & -\lambda_3 - \lambda_{-2} & \lambda_{-3} \\ \lambda_{-4} & 0 & \lambda_3 & -\lambda_4 - \lambda_{-3} \\ 1 & 1 & 1 & 1 \end{pmatrix}\begin{pmatrix} P_A \\ P_B \\ P_C \\ P_D \end{pmatrix} = \begin{pmatrix} 0 \\ 0 \\ 0 \\ 0 \\ 1 \end{pmatrix}.$$

The solution of this system is $(P_A, P_B, P_C, P_D) = (1/\beta)(1, \Lambda_1, \Lambda_1\Lambda_2, \Lambda_1\Lambda_2\Lambda_3)$.

We can now use the P_i to approximate the mean number of transitions between each state. As an example, consider the mean number of transitions between state $i = A$ and state $i = B$. The total amount of time the particle spends in state A is $\langle t\rangle P_A$. The particle transitions out of state A into state B or D with a total rate $\lambda_1 + \lambda_{-4}$ and therefore the number of transitions is $\langle t\rangle P_A(\lambda_1 + \lambda_{-4})$. We can calculate how many of these transitions were strictly to state B by noting that the probability of transitioning, given that a transition occurred, from A to B is $\lambda_1/(\lambda_1 + \lambda_{-4})$. Therefore, the number of transitions from A to B is $[\langle t\rangle P_A(\lambda_1+\lambda_{-4})][\lambda_1/(\lambda_1+\lambda_{-4})] = \lambda_1\langle t\rangle P_A$. A similar calculation shows that hits $(B \to A) =$ hits $(A \to B)$. In this way we can estimate the mean number (#) of transitions along any arrow in the reaction network, while the particle (pMHC) stays in the cluster:

$$\#(A \rightleftharpoons B) = \lambda_1\langle t\rangle P_A, \tag{7a}$$
$$\#(B \rightleftharpoons C) = \lambda_2\langle t\rangle P_B, \tag{7b}$$
$$\#(C \rightleftharpoons D) = \lambda_3\langle t\rangle P_C, \tag{7c}$$
$$\#(D \rightleftharpoons A) = \lambda_4\langle t\rangle P_D. \tag{7d}$$

RESULTS

TCR/pMHC binding events in a mobile TCR cluster

We begin our study of the TCR/pMHC dynamics by focusing on a single TCR cluster that forms in the pSMAC and travels toward the cSMAC. We first calculate an upper bound on the number of TCR a pMHC can hit (bind to) during one visit to that cluster. Yokosuka et al. (19) experimentally measured the mean velocity of 81 TCR clusters as a function of their initial formation location. They found a mean velocity of $V =$ 0.0249 μm/s for pSMAC clusters traveling toward the

cSMAC and found that these clusters migrated a maximum of $L_{max} = 4.5\ \mu$m toward the cSMAC (Fig. S1 in their work). Therefore the maximum journey time is $t_{max} \approx 181$ s. If, during this time, a pMHC molecule can continually engage TCR (i.e., the pMHC molecule cannot escape the cluster) and the mean time for a free pMHC to bind a TCR is negligible (i.e., the reaction on-rate is very large), then the number of TCR engagements, or hits, can be approximated by dividing t_{max} by the mean TCR-pMHC bond lifetime, $1/k_{off}$. Typical off-rates for agonist pMHC are 0.03–0.3 s^{-1} (1), and therefore the maximum number of possible hits, if the pMHC remains in the cluster for 181 s is in the range of ~5–54.

This rough calculation suggests that, in principle, a single pMHC molecule can engage a substantial number of TCR in a cluster before arriving at the cSMAC. However, the number of engagements can be significantly reduced by considering the effects of pMHC diffusion, TCR cluster composition and mobility, and the finite reaction on-rate. In the next section we will use our escape time formulation to quantify the decrease in the number of hits when these effects are considered.

Two-state escape time formulation from a mobile TCR cluster

To investigate the behavior of a single pMHC within a mobile TCR cluster, we consider the pMHC to be in one of two states; unbound ($i = $ A) or bound ($i = $ B) to a TCR; see Fig. 2 (basic model). The reaction scheme is $A \rightleftharpoons B$, with a forward rate λ_1, backward rate λ_{-1}, and transition affinity $\Lambda_1 = \lambda_1/\lambda_{-1}$.

We define the number of hits for this simple model to be the number of times (on average) the pMHC binds a TCR during its time in the cluster. We compute the mean escape time, the pMHC transport distance, and the number of hits by reducing the four-state model described earlier to a two-state model. This reduction is achieved by setting $\Lambda_2 = \Lambda_3 = \Lambda_4 = 0$ in Eqs. 6 and 7a. The number of hits in this two-state model is then

$$\text{hits}(A \rightleftharpoons B) = \langle t \rangle \frac{\lambda_1}{1 + \Lambda_1}. \quad (8)$$

We plot the mean escape time, t_A, as a function of the initial position of the pMHC in Fig. 3 for different values of V. We find that microcluster velocities $<0.1\ \mu$m/s do not significantly affect the escape time.

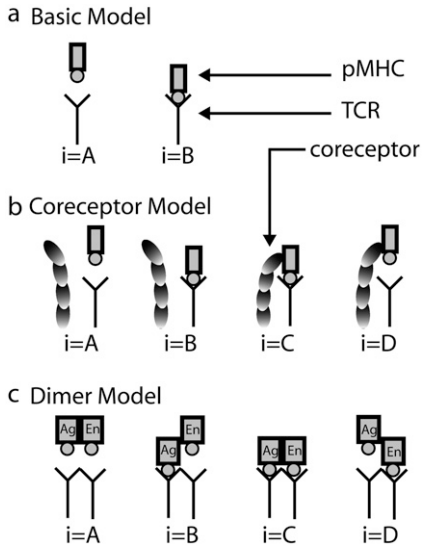

FIGURE 2 Reactions schemes we consider. (*a*) Two-state reaction scheme between single pMHC and TCR. Inclusion of coreceptors (*b*) or dimeric pMHC molecules (*c*) requires a four-state reaction scheme. Ag = agonist pMHC; En = endogenous (nonstimulatory) pMHC.

Estimating the pMHC transport distance and total TCR engagements

Before we can determine the number of TCR engagements by a pMHC molecule in a cluster we need to estimate parameters. Several recent studies have characterized TCR cluster composition and mobility (19–21). By comparing background and cluster anti-TCR-fab fluorescence intensity, Campi et al. (20) determined that 140 TCR are contained in a single cluster. Consistent with these findings, Yokosuka et al. (19) reported 40–150 CD3ζs per cluster. Cluster area was observed to be 0.35–0.5 μm^2 (20). The concentration range of TCR in a cluster is then $T_{mc} = 80$–$430\ \mu m^{-2}$. We also take the diffusion coefficient of pMHC to be $D_P = 0.03\ \mu m^2/s$ (13). These parameters are summarized in Table 1.

We summarize experimentally determined reaction rates between various TCR and pMHC in Table 2. The transition rates in our model are related to these using the relations

$$\lambda_1 = \overline{k}_{on} T_{mc},\ \lambda_{-1} = k_{off}, \quad (9)$$

where $\overline{k}_{on}$ is the two-dimensional on-rate which can be related to the experimentally measured three-dimensional

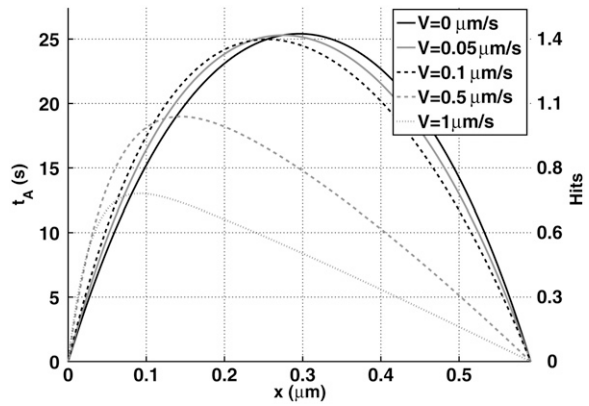

FIGURE 3 Residence time in a TCR cluster as a function of initial position. We plot $t_A(x, y)$ as a function of x for $y = b/2$ for several values of the microcluster velocity V. We use reaction parameters for the MCC88-103 peptide (Table 2): $b = 0.59\ \mu$m, $T_{mc} = 286\ \mu m^{-2}$, $D_P = 0.03\ \mu m^2/s$, $\overline{k}_{on} = 0.0057\ \mu m^2/s$ and $k_{off} = 0.057\ s^{-1}$.

TABLE 1 Parameter definitions and estimations

Parameter	Description	Reported parameter ranges
A_{mc}	TCR microcluster area	0.35–0.5 μm^2 (20)
b	TCR microcluster dimension	$A_{mc} = b^2$, $b = 0.59 - 0.71$ μm or $A_{mc} = \pi b^2$, $b = 0.33 - 0.40$ μm
R	Synapse radius	5–6 μm
N_T	TCR number in a microcluster	40–150 (19,20)
T_{mc}	TCR concentration in microclusters	80–430 μm^{-2}
T_0	TCR concentration outside microclusters	50 μm^{-2}
C_{mc}	Coreceptor concentration in microclusters	Not known
K_D	TCR/pMHC dissociation constant	0.005–1500 μM (see Table 2)
K_D^C	Coreceptor/pMHC dissociation constant	~200 μM (32,36)
V	TCR microcluster velocity	0.0249 μm/s (19)
D_P	pMHC diffusion coefficient	0.03 μm^2/s (13,49)

on-rate using a confinement length (Table 2) (27,28). The two-dimensional forward rate constant $\overline{k}_{on}$ for the peptide MCC88-103 was calculated from its k_{off} value and the two-dimensional dissociation constant determined in Grakoui et al. (1). For the other peptides, $\overline{k}_{on}$ was calculated by assuming that the proportionality constant was the same as for MCC99-103. In relating the transition rates to the reaction rates in this way (Eq. 9) we have assumed that there is no competition among pMHC for TCR. This assumption is reasonable because pMHC concentration is low (<10 μm^{-2}) compared to the cluster TCR concentration (>100 μm^{-2}).

We can now compute the mean escape time $\langle t \rangle$ (Eq. 6, $\beta = 1 + \Lambda_1$), pMHC transport distance $\langle L \rangle$, and total hits (using Eq. 8). We summarize these three results for specific TCR and pMHC in the CR^- columns of Table 2. We can draw two main conclusions:

1. pMHC interactions with TCR in a mobile cluster are insufficient to consistently transport pMHC to the cSMAC in a single journey ($\langle L \rangle < 4.5$ μm).
2. Most pMHC molecules engage <5 TCR in the cluster.

However, exceptions to these conclusions exist. For example, clusters comprised of 172.10 TCR transport MBP1-11 to the cSMAC and MBP1-11 can engage 40 TCR. There are also examples of substantial TCR engagement even though the pMHC is not transported to the cSMAC (e.g., 172.10/MBP1-11, JM22z/HLFA-A2).

In constructing Table 2 we have imposed the total journey time, $t_{max} = 181$ s, as an upper limit to $\langle t \rangle$, which subse-

TABLE 2 Estimates of TCR hits and pMHC transport by a mobile TCR cluster

						$\langle t \rangle$ (s)		$\langle L \rangle$ (μm)		Hits	
TCR	pMHC	K_D (μM)	k_{on} (M^{-1} s^{-1})	$\overline{k}_{on}$ (μm^2 s^{-1})	k_{off} (s^{-1})	CR^-	CR^+	CR^-	CR^+	CR^-	CR^+
Data from Grakoui et al. (1)											
2B4	MCC88-103	60.2	900	0.0057	0.057	12	121	0.30	3.0	0.67	6.7
2B4	T102S	238	1500	0.0095	0.36	3.5	35	0.087	0.87	1.1	11
2B4	T102G	1520	3400	0.022	5.0	0.91	9.2	0.023	0.23	2.5	25
3.L2	Hb64-76	12.1	5557	0.035	0.064	65	180	1.6	4.5	4.1	12
3.L2	N72T	9.90	15,374	0.097	0.136	84	181	2.1	4.5	11	25
3.L2	N72I	14.9	16,600	0.11	0.248	50	181	1.2	4.5	12	45
Data from Krogsgaard et al. (50)											
2B4	102S	90	2240	0.014	0.20	8.7	87	0.22	2.2	1.7	17
2B4	PCC	32	1080	0.0068	0.035	23	181	0.58	4.5	0.80	6.2
2B4	MCC95-103	8.7	2200	0.014	0.019	86	181	2.1	4.5	1.6	3.4
2B4	K2	8.7	6670	0.042	0.058	86	181	2.1	4.5	4.9	10
2B4	K3	33	2120	0.013	0.071	23	181	0.56	4.5	1.6	12.6
2B4	K5	2.9	4900	0.031	0.014	181	181	4.5	4.5	2.5	2.5
Data from Garcia et al. (51)											
172.10	MBP1-11	5.9	37,200	0.24	0.219	126	181	3.1	4.5	28	39
1934.4	MBP1-11	31	5130	0.032	0.160	24	181	0.60	4.5	3.8	28
Data from Willcox et al. (52)											
JM22z	HLFA-A2	17	69,000	0.44	1.2	43	181	1.1	4.5	51	215

We calculate $\langle t \rangle$, $\langle L \rangle$, and hits as described in the main text in the absence (CR^-) and presence (CR^+) of coreceptors. The three-dimensional molar values are converted to two-dimensional values using a confinement length of 0.262 μm (13). Parameters: $b = 0.59$ μm, $T_{mc} = 100$ TCR/$(0.59$ $\mu m)^2 = 286$ μm^{-2}, $C_{mc} = T_{mc}$, $K_D^C = 200$ μM, $V = 0.0249$ μm/s, and $D_P = 0.03$ μm^2/s.

quently imposes an upper bound on $\langle L \rangle$ and hits. We impose this upper bound because once in the cSMAC, TCR begin to be internalized (21), an effect not accounted for in our model. We also focus on the cluster journey because experiments have shown that pMHC-dependent signaling through the TCR occurs during the journey to the cSMAC and not in the cSMAC itself (19–21,29).

We can also determine the required TCR/pMHC affinity to achieve pMHC transport to the cSMAC by a single mobile cluster from Eq. 6. Using the parameters given above, we calculate $\langle \Phi \rangle = 0.41$ s (Eq. 4). Setting $\langle t \rangle = t_{max}$, we find that, on average, the pMHC remains in the microcluster for t_{max} provided $\beta > 442.2$. For a TCR concentration of $T_{mc} = 286$ μm^{-2} this corresponds to $\overline{K}_D < 0.65$ μm^{-2}. The maximum three-dimensional dissociation constant that permits transport to the cSMAC, based on the TCR-pMHC interaction alone is, therefore, $K_D^* = 4.1$ μM.

We note that estimates of TCR numbers in clusters and estimates of cluster size, discussed above, rely on optical fluorescence microscopy (19,20). Since clusters cannot be resolved by optical microscopy, the latter estimate is probably an upper bound. We find that variations in cluster size do not have a significant effect on $\langle t \rangle$ and hits, provided we fix the number of TCR per cluster, because a decrease (increase) in cluster size is proportionally balanced by a larger (smaller) reaction on-rate.

Coreceptors augment TCR/pMHC interactions

There is a growing body of evidence suggesting that T cell activation by pMHC molecules is dependent upon coreceptors CD4 (1,5,30,31) or CD8 (12,22,32,33). In cases where the pMHC concentration is low (1,5,35) or the pMHC exhibits small affinity to TCR (12), T cells lacking coreceptors have been observed to be less likely to form an immune synapse (1,5), flux calcium (5,35), proliferate (1), or secrete IL-2 (12). How coreceptors facilitate the activation of T cells remains largely unknown, in part because the experimentally determined affinity between CD4 or CD8 and MHC is very weak ($K_D \sim 200$ μM) (32,36) (reviewed in (37)). CD4 and CD8 are known to associate with TCR via the signaling molecules Lck and ZAP-70 (38,39), possibly providing additional stabilization to the TCR-pMHC-coreceptor complex.

In this section we will show that coreceptors, although having weak binding to MHC, sufficiently augment the TCR/pMHC interactions such that substantial TCR engagement and pMHC transport to the cSMAC are achieved.

Four-state escape time formulation from a mobile TCR cluster

To determine the degree to which coreceptors augment the TCR/pMHC interaction we will need to consider the full four-state escape time problem. In this reaction scheme, the pMHC molecule can exist in four states: unbound from both TCR and coreceptor ($i = A$), bound to TCR ($i = B$), bound to TCR and coreceptor ($i = C$), and bound to a coreceptor ($i = D$), see Fig. 2 (coreceptor model). There are two fundamental reactions in this scheme: TCR/pMHC (transition rates: λ_1,λ_{-1}) and coreceptor/pMHC (transition rates: λ_2, λ_{-2}). We assume the reactions occur independently and therefore identify the transitions between states C and D with those of A and B (i.e., $\lambda_{-3} = \lambda_1$, $\lambda_3 = \lambda_{-1}$) and transitions between states D and A with those of B and C (i.e., $\lambda_{-4} = \lambda_2$, $\lambda_4 = \lambda_{-2}$).

As before, the mean escape time is given by Eq. 6, with $\beta = (1 + \Lambda_1)(1 + \Lambda_2)$ in this case. We also keep track of the total number of times the pMHC binds TCR or ''hits'' (in this case determined by summing Eqs. 7a and 7c. The P_i in Eqs. 7a–7d can be simplified to the form

$$\begin{pmatrix} P_A \\ P_B \\ P_C \\ P_D \end{pmatrix} = \frac{1}{\beta} \begin{pmatrix} 1 \\ \Lambda_1 \\ \Lambda_1\Lambda_2 \\ \Lambda_2 \end{pmatrix}. \quad (10)$$

Coreceptors increase pMHC transport distance and total hits

The only additional parameter we introduce by including coreceptors is their transition affinity for the MHC molecule, Λ_2. This parameter is related to the equilibrium dissociation constant as follows,

$$\Lambda_2 = C_{mc}/\overline{K}_D^C, \quad (11)$$

where C_{mc} is the coreceptor concentration in the cluster and $\overline{K}_D^C$ is the two-dimensional dissociation constant between pMHC and coreceptors. The three-dimensional dissociation constant has been reported to be $\sim$200 μM between class I MHC and CD8$\alpha\alpha$ (32) and $\sim$199 μM between class II MHC and CD4 (36). As before, we convert three-dimensional values to two-dimensional values using a confinement length (see Table 2).

The results when coreceptors are incorporated into the TCR/pMHC model are summarized in the CR^+ columns of Table 2. We find that in most cases, the addition of coreceptors maximizes the mean escape time resulting in pMHC transport to the cSMAC. Furthermore, pMHC molecules that exhibit few TCR engagements in the absence of coreceptors are able to engage a substantial number of TCR in the presence of coreceptors. These increases are observed despite the large dissociation constant for the coreceptor-MHC interaction.

T cell stimulation is correlated to pMHC transport to cSMAC

The importance of coreceptors to T cell stimulation was highlighted in a study by Holler and Kranz (12). Briefly, they

measured IL-2 release after interactions between APC bearing a particular pMHC and $CD8^-$ or $CD8^+$ T cells. In separate experiments, they determined the binding constants for some of the TCR-pMHC pairs in their experiments. They found that coreceptors were necessary for T cell stimulation only when the dissociation constant for the TCR/pMHC bond roughly exceeded 5 μM. This is comparable to our previous estimate for the minimal affinity required to retain pMHC within a TCR cluster for travel to the cSMAC (described above) of 4.1 μM.

In Table 3 we summarize the reaction rates for TCR/pMHC combinations used in their study and indicate the particular experiments where coreceptors were required for T cell stimulation. In this table we also compute $\langle t \rangle$, $\langle L \rangle$, and total hits in the absence (CR^-) and presence (CR^+) of coreceptors. We find a striking correlation between the experimental determination of CD8 dependence and our theoretical determination of whether the pMHC can be expected to travel to the cSMAC. We also find that, if T cell stimulation is independent of CD8, the predicted number of hits is also independent of the presence of coreceptors, but the opposite is true when CD8 is required for T cell stimulation.

We can write a simple formula to estimate the maximum pMHC-TCR dissociation constant, K_D^*, that gives pMHC transport to the cSMAC. Rearranging $\beta = (1 + \Lambda_1)(1 + \Lambda_2)$ and substituting the physical parameters for Λ_1 and Λ_2 we obtain

$$\overline{K}_D^* = \frac{T_{mc}(\overline{K}_D^C + C_{mc})}{\beta \overline{K}_D^C - (\overline{K}_D^C + C_{mc})}. \quad (12)$$

We obtain $\overline{K}_D^* = 6.65\ \mu m^{-2}$ (using parameters $\beta = 442.2$, $\overline{K}_D^C = 31.6\ \mu m^{-2}$, and $C_{mc} = T_{mc} = 286\ \mu m^{-2}$). The three-dimensional value is then $K_D^* = 42.1\ \mu$M, an order-of-magnitude larger than in the case without coreceptors. Examining Tables 2 and 3 we can see that many TCR/pMHC have a lower K_D than this, permitting pMHC transport and maximal hits when coreceptors are present.

In our analysis of the effects of coreceptors on pMHC transport and TCR hits we have assumed equal concentrations of coreceptors and TCR. Lower concentration of coreceptors would decrease K_D^*. In Fig. 4 we plot K_D versus K_D^C using Eq. 12 for $C_{mc} = [T_{mc}, T_{mc}/2, T_{mc}/5, T_{mc}/10]$. We find that at lower coreceptor concentration, a dissociation constant of $\sim$200 μM is too large to achieve pMHC transport to cSMAC. We conclude that if coreceptors facilitate pMHC transport to the cSMAC, they must be present in clusters at concentrations comparable to that of TCR.

Potential effects of pMHC dimers on the APC

Biochemical assays have provided evidence that MHC class II molecules form dimers (40,41) and it is reasonable to suppose that they may form dimers in experiments using supported bilayers or APC. pMHC dimers have also been shown to be the minimal unit required for T cell activation in an assay where soluble multimeric pMHC complexes were used to stimulate T cells (42), although it is not clear to what extent this result informs the physiological situation where binding occurs at a cell-cell interface. Furthermore the coreceptor and the TCR that it associates with may bind different pMHC complexes (31,43). This forms a ''pseudodimer'' model of TCR triggering, proposed in part to explain the observation that a single agonist pMHC complex can lead to TCR triggering. It was suggested that, when a TCR with an associated coreceptor binds to an agonist-pMHC, the coreceptor binds a distinct self/null-pMHC complex. A TCR pseudodimer is formed when a second TCR binds to this self-pMHC complex.

We will show that pMHC dimers can boost the effective affinity of their constituent pMHC for the cluster and thus allow enhanced pMHC transport to the cSMAC. Therefore,

TABLE 3 CD8 augments low-affinity TCR/pMHC interactions

						$\langle t \rangle$ (s)		$\langle L \rangle$ (μm)		Hits	
TCR	pMHC	K_D (μM)	k_{on} ($M^{-1}\ s^{-1}$)	$\overline{k}_{on}$ ($\mu m^2 s^{-1}$)	k_{off} (s^{-1})	CR^-	CR^+	CR^-	CR^+	CR^-	CR^+
T cell stimulation is CD8-independent											
2C	QL9/L	3.9	6300	0.040	0.025	181	181	4.5	4.5	4.5	4.5
m6α	QL9/L	0.0055	155,000	0.98	0.0008	181	181	4.5	4.5	0.15	0.15
m6α	Y5/L	0.0051	115,000	0.73	0.0006	181	181	4.5	4.5	0.11	0.11
m6α	M5/L	0.034	147,000	0.93	0.005	181	181	4.5	4.5	0.90	0.90
m6α	H5/L	0.0778	NA	—	NA	181	181	4.5	4.5	—	—
m6α	Q5/L	0.167	NA	—	NA	181	181	4.5	4.5	—	—
m67α	SIYR/K	0.0159	277,000	1.75	0.44	181	181	4.5	4.5	79	79
T cell stimulation is CD8-dependent											
2C	dEV8/K	84.1	2200	0.014	0.185	9.2	92	0.24	2.3	1.6	16
m33α	dEV8/K	38	NA	—	NA	20	181	0.49	4.5	—	—
m67α	dEV8/K	6.57	86,000	0.54	0.567	113	181	2.8	4.5	64	102
2C	SIYR/K	31.9	2300	0.015	0.075	23	181	0.58	4.5	1.7	13

Data taken from Holler and Kranz (12). Calculations and parameters are described in Table 2.

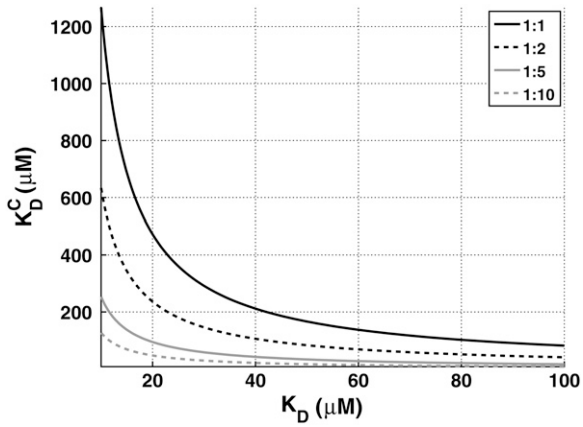

FIGURE 4 Maximum dissociation constant (K_D^C) of coreceptors required to achieve transport of agonist pMHC to cSMAC. The dissociation constant between the agonist pMHC and TCR is given on the x axis (K_D). Results are shown for different ratios of coreceptor/TCR in the microcluster.

higher-order complexes such as pseudo-dimers will also allow enhanced transport.

To study the effects of pMHC dimers we use the full four-state escape time formulation; see Fig. 2 (dimer model). This is exactly analogous to the coreceptor theory, with Λ_2 in this case related to the second pMHC molecule in the pMHC dimer,

$$\Lambda_2 = T_{mc}/\overline{K}_D^{(2)}, \tag{13}$$

where $K_D^{(2)}$ is the dissociation constant for the TCR-second pMHC bond. In the case of homodimers (identical presented peptide and MHC molecule), we ignore any cooperative effects and set $K_D^{(2)} = K_D$. In the case of heterodimers, $K_D^{(2)}$ will be different from K_D.

As in the previous cases, we find a simple relationship to determine the maximum dissociation constant, K_D*, required for pMHC transport to the cSMAC. Using the definition of β we find

$$\overline{K}_D^* = \frac{T_{mc}(\overline{K}_D^{(2)} + T_{mc})}{\beta\overline{K}_D^{(2)} - (\overline{K}_D^{(2)} + T_{mc})}. \tag{14}$$

This equation is equivalent to Eq. 12 when $C_{mc} = T_{mc}$ and is shown in Fig. 4 (1:1 case). In the case of pMHC homodimers, we find that for $K_D < 80$ μM the dimer will be transported to the cSMAC. Consequently, transport to the cSMAC is expected for almost all homodimers of pMHC listed in Tables 2 and 3.

The observation that endogenous peptides accumulate in the IS (35) and that heterodimers of agonist/endogenous pMHC stimulate T cells (43) suggest that endogenous peptides may play a role in pMHC transport to the cSMAC and in serial triggering. Endogenous peptides generally have an undetectable affinity for TCR and therefore have a dissociation constant >200 μM. Equation 14 (shown in Fig. 4, 1:1 case)) indicates that endogenous peptides are able to transport the heterodimer only when the dissociation constant of the agonist peptide is stronger than ~40 μM. In cases when the agonist pMHC dissociation constant is >40 μM, we predict that the addition of endogenous peptides alone will not sufficiently augment the interaction to result in pMHC transport to the cSMAC and substantial serial engagement of TCR.

TCR/pMHC binding events with multiple TCR clusters

In the previous sections we have shown that agonist pMHC can be expected to escape from TCR clusters during the journey to the cSMAC unless the reaction is augmented by coreceptors or pMHC dimers. Substantial TCR engagements and transport to the cSMAC could be possible in the absence of these factors if a single pMHC molecule visits multiple TCR clusters whose collective motion sieves the pMHC molecules into the cSMAC.

We leave a complete examination of pMHC dynamics in a field of moving clusters for future work, focusing here on the question of how many engagements (hits) a pMHC would experience during a single sojourn in an IS that holds a number of immobile clusters enriched in TCR as well as a background concentration of nonclustered TCR. Varma et al. (21) generated such synapses by treating T cells with latrunculin-A, a cytoskeleton poison, shortly after synapse formation. The result, shown in Fig. 6, *F–J*, of their work, is an immobile and stable field of TCR clusters. In Fig. 3, *C* and *D*, of their work, they also illustrate the rapid (~60 s) reduction in calcium signaling upon administrating latrunculin-A to T cells forming an IS. To form a clear picture of the potential effects of multiple TCR clusters, in what follows we will not include coreceptors.

We reduce system 1 by setting $\lambda_{\pm i} = 0$, for all $i \neq 1$, and removing the advective field by setting $\vec{V}_i = 0$, for all i. We take the synapse to be a disk of radius R containing N disk-shaped clusters centered at the points $\mathbf{r}_1, \mathbf{r}_2, \ldots \mathbf{r}_N$ and having a radius of b. Each cluster contains N_T TCR. These simplifications allow us to write a single equation governing the escape time t^{syn},

$$D_P\nabla^2 t^{syn} = -1 - \frac{\lambda_1}{\lambda_{-1}}I(\mathbf{r}) - \frac{\lambda_1^*}{\lambda_{-1}}(1 - I(\mathbf{r})), \tag{15}$$

$$I(\mathbf{r}; \mathbf{r}_1, \mathbf{r}_2, \ldots \mathbf{r}_N) = \begin{cases} 1 & |\mathbf{r} - \mathbf{r}_j| \leq b \\ 0 & |\mathbf{r} - \mathbf{r}_j| > b \end{cases}, \tag{16}$$

where the superscript, *syn*, indicates the escape time is from the entire synapse. The boundary condition is $t^{syn} = 0$ when $|\mathbf{r}| = R$. To account for the difference between background and clustered TCR concentrations, we have split the reaction term into two parts using the indicator function I, which is zero everywhere except within clusters where it is equal to one. Therefore the term with λ_1/λ_{-1} captures reactions within clusters having a forward transition rate λ_1. The term with λ_1*/λ_{-1} captures reactions outside of clusters with a forward rate

λ_1*. The transition rates are related to the physical parameters by Eq. 9 and the relation $\lambda_1^* = \bar{k}_{on} T_0$ where T_0 is the TCR concentration outside clusters, which we take to be 50 μm^{-2} (19). The TCR concentration within clusters is $N_T/(\pi b^2)$.

As discussed earlier, there is uncertainty in the amount of area covered by TCR in clusters. Consequently, in the analysis that follows we fix the number of TCR per cluster, N_T, and vary the cluster size, b. We can decompose the solution to Eq. 15 into three parts, $t^{syn} = t_1 + t_2 + t_3$, satisfying

$$D_P \nabla^2 t_1 = -1, \tag{17a}$$

$$D_P \nabla^2 t_2 = -\frac{\lambda_1}{\lambda_{-1}} I(\mathbf{r}), \tag{17b}$$

$$D_P \nabla^2 t_3 = -\frac{\lambda_1^*}{\lambda_{-1}} (1 - I(\mathbf{r})). \tag{17c}$$

All the $t_i = 0$ on the synapse boundary (i.e., $t_i(r = R) = 0$). The expression $t_1(r) = (R^2 - r^2)/(4D)$ is the escape time from a synapse without any TCR, leading to the average time of escape $\langle t_1 \rangle = R^2/8D_P$ (averaged over all possible starting positions). The value t_2 is the time spent bound to clustered TCR, and t_3 is the time spent bound to nonclustered TCR. By linearity, $t_3 = (\lambda_1^*/\lambda_{-1})t_1 - (\lambda_1^*/\lambda_1)t_2$. Substituting in for the physical parameters, we obtain $t_3 = (T_0 \bar{k}_{on}/k_{off})t_1 + (T_0 \pi b^2/N_T)t_2$. This shows that $t_3 \approx (T_0 \bar{k}_{on}/k_{off})t_1$ as $b \to 0$, in agreement with the theory for a uniform distribution of TCR presented in Wofsy et al. (13). We can obtain the mean number of transitions in this case by dividing the total time spent bound to TCR, $t_2 + t_3$, by the mean time per binding event, $1/\lambda_{-1}$ (i.e., hits $= \lambda_{-1} \langle t_2 + t_3 \rangle$).

Weak dependence of escape time on cluster size

If $b/R \ll 1$ then we can use matched asymptotics to obtain t_2 as a power series in the small parameter $\epsilon = b/R$ (see Appendix). Averaging over all starting positions of the pMHC, we find, to first order in ϵ,

$$\langle t_2 \rangle = \frac{\bar{k}_{on} N_T}{4\pi k_{off} D_P} \sum_{k=1}^{N} \left(1 - \left|\frac{\mathbf{r}_k}{R}\right|^2\right), \tag{18}$$

$$\langle t^{syn} \rangle = \left(1 + \frac{T_0 \bar{k}_{on}}{k_{off}}\right)\frac{R^2}{8D_P} + \left(1 - \frac{T_0 \pi b^2}{N_T}\right)\frac{\bar{k}_{on} N_T}{4\pi k_{off} D_P} \times \sum_{k=1}^{N} \left(1 - \left|\frac{\mathbf{r}_k}{R}\right|^2\right). \tag{19}$$

We see that, to first order in ϵ, $\langle t^{syn} \rangle$ depends only on physical parameters and the locations of the clusters relative to the synapse boundary, and that centrally located clusters have the biggest impact on the mean time a pMHC spends in the synapse.

We can also consider the case where we assume that the pMHC starts within a cluster. In this case, we average over all possible starting positions within clusters to obtain the mean time spent bound to clustered TCR,

$$\langle t_2^{in} \rangle = \frac{N_T \bar{k}_{on}}{\pi k_{off} D_P}\left[\frac{1}{8} - \frac{\log(b/R)}{2} + \frac{1}{N}\sum_{j=1}^{N} A_{j,0}\right], \tag{20}$$

where the $A_{j,0}$ are constants that depend only on the cluster positions (see Appendix). This formulation reveals the weak (logarithmic) dependence of escape time on TCR cluster size, b.

pMHC engagement of clustered TCR is nearly independent of cluster size

We begin by randomly placing TCR clusters within a synapse of radius 5.5 μm. In Fig. 5 *a* we show the locations, $\mathbf{r}_j$, of $N = 5$ (*black*), $N = 25$ (*black + dark gray*), and $N = 50$ (all disks) TCR clusters. In Fig. 5 *b* we plot the total hits to clustered TCR (*solid line*) and to nonclustered TCR (*dashed line*) as a function of b for the three values of N. We obtain $\langle t_2 \rangle$, and hence the total hits, by using a central difference scheme for the Laplacian in Eq. 17 when $b > 0.07$ μm. When $b < 0.1$ μm we use the asymptotic solution, Eq. 18, which agrees with the numerical solution on the overlapping range of b. We take reaction rates for a typical TCR-pMHC interaction: $\bar{k}_{on} = 0.05$ $\mu m^2/s$, $k_{off} = 0.05$ s^{-1}.

We find that the total hits to clustered TCR increases with N but is independent of the cluster size. Indeed, the asymptotic solution, Eq. 18, is independent of b. As $b \to 0$, for all values of N, the total hits to TCR external to clusters asymptotes to the value it would have if there were no clusters, as it should. For larger values of b, the total hits to nonclustered TCR decreases as N increases. The small changes in the number of hits at large $b \simeq 1$ μm occur because, in the simulation, parts of the microclusters end up outside the idealized synapse region.

As discussed earlier, Varma et al. (21) created synapses containing immobile TCR clusters. To obtain a physiological TCR microcluster distribution, we performed simple image analysis on Fig. 6 *H* of their work. We acquired a high resolution version of their Fig. 6 *H* and performed thresholding to convert the grayscale total internal reflection fluorescence image into a binary (black/white) image. Morphological open and close operations were performed to remove isolated pixels. The resulting TCR microcluster stencil, shown in Fig. 5 *c*, was used as the indicator function for a numerical solution of Eq. 17. The synapse boundary, where $t_i = 0$, was obtained by alternate thresholding and multiple morphological open operations on the total internal reflection fluorescence image (see *black outline* in Fig. 5 *c*).

To examine the effect of cluster size we use a morphological operation that removes pixels that are not surrounded. Applying this morphological operation multiple times on the TCR cluster stencil progressively decreases the total TCR cluster area. We show the TCR cluster stencil at three instances in Fig. 5 *c*. We keep the total number of TCR in clusters fixed at 5000, equivalent to 100 TCR distributed

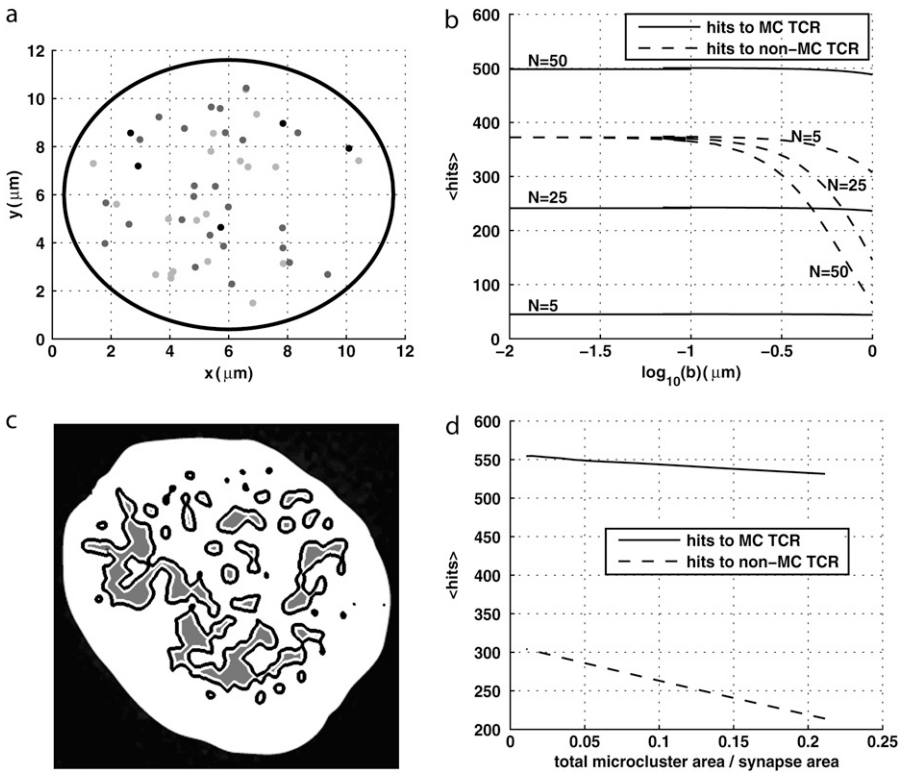

FIGURE 5 Number of pMHC engagements to clustered TCR is almost independent of cluster size. We compute the number of binding events (hits) in two scenarios. In panel *a*, we use an idealized disk synapse of radius 5.5 μm containing N randomly distributed TCR microclusters each of radius b and containing $N_T = 100$ TCR. The positions of $N = 5$ (*black*), $N = 25$ (*black + dark gray*), and $N = 50$ (all disks) TCR clusters is shown. In panel *b*, we use the TCR microcluster distribution from panel *a* to compute the total hits to clustered (*solid line*) and nonclustered (*dashed line*) TCR for the three values of N as a function of the microcluster size, panel *b*. In panel *c*, we use experimental data (Fig. 6 *H* in (21)) to obtain a physiological microcluster distribution, see main text for details. Also shown in panel *c* are three steps along the multiple erosion operations performed on the microcluster stencil. Using these microcluster distributions we compute the total hits (*d*) as a function of the total microcluster area. Parameters: $\bar{k}_{on} = 0.05\ \mu m^2/s$, $k_{off} = 0.05\ s^{-1}$, and $D_P = 0.03\ \mu m^2/s$.

across 50 clusters ($N = 50$ in the idealized synapse). We take $\overline{k}_{on}$, k_{off}, and D_P as in the idealized synapse calculation. In Fig. 5 *d* we plot the total hits as a function of the microcluster to synapse area ratio (synapse area is fixed at 85 μm^2). The total hits to clustered TCR remains almost unchanged.

The main trend observed in Fig. 5, that the number of hits to clustered TCR is only weakly dependent on cluster size, is a result of keeping the number of TCR per cluster constant. Decreases in cluster area are balanced by increases in the reaction on-rate within clusters leaving the number of hits unchanged. The number of hits that a single pMHC makes with clustered and nonclustered TCR during a single sojourn in the IS is substantial, even without the aid of bond stabilization by coreceptors or dimerization.

DISCUSSION

Experimental observations show pMHC-dependent signaling in TCR clusters and the accumulation of pMHC in the cSMAC. Using a series of mathematical models we have analyzed serial engagement of TCR and transport of pMHC by mobile TCR clusters. We have shown that the TCR-pMHC interaction alone does not support substantial serial engagement of TCR or pMHC transport to the cSMAC by a single cluster but that if the TCR-pMHC bond can be stabilized (for instance, by coreceptor molecules such as CD4/8 or by dimerized pMHC, or by combined effects thereof), transport to the cSMAC and serial engagement within a single cluster can be expected. We have calculated minimum affinities of the TCR-pMHC bond that allow pMHC transport to the cSMAC to proceed efficiently in each scenario. We found evidence that coreceptors CD4/8 must be present in concentrations comparable to that of clustered TCR for pMHC transport in a coreceptor-dependent manner. Using experimental data (12) we were able to correlate predicted pMHC transport to the cSMAC with T cell stimulation as measured by IL-2 production. We also analyzed the role of multiple clusters in trapping pMHC in the synapse and boosting serial engagement. Our conclusions are based on a number of modeling assumptions and suggest future directions of experimental and theoretical enquiry. We discuss these in turn.

Parameter estimation

Our results underline the importance of measuring the kinetic parameters for TCR-pMHC bonds. The parameters which have the largest uncertainty in our model are probably the two-dimensional dissociation constant, $\overline{K}_D$, and two-dimensional on-rate, $\overline{k}_{on}$. We obtained two-dimensional values by converting their respective experimentally measured three-dimensional values using a constant factor (confinement length) determined for a specific TCR/pMHC interaction. In a review, Davis et al. (6) discuss the importance of directly determining two-dimensional rates, as they can be substantially different from their respective three-dimensional values. Recently, we have proposed a method to directly determine two-dimensional affinities and on-rates

using live cells based on fluorescence recovery after photobleaching (53).

In this article we used the macroscopic or long-range diffusion coefficient for pMHC which can be substantially smaller than the microscopic diffusion coefficient (44). Increases in D_P would decrease our predictions of $\langle t \rangle$, pMHC transport distance, and hits. We also remark that we have assumed that pMHC binding to TCR creates TCR-pMHC complexes that cannot diffuse. Diffusion of these complexes within the cluster would also decrease $\langle t \rangle$. In the absence of other uncertainties concerning the binding parameters, these considerations would mean that the values of $\langle t \rangle$ in Tables 2 and 3 would be upper bounds. Fluorescence recovery after photobleaching experiments could indicate the extent to which diffusion constants change after TCR-pMHC binding.

Role of clusters in TCR signaling

Our calculations of numbers of TCR-pMHC engagement (i.e., hits) in single clusters are smaller than those calculated for a homogeneous TCR distribution (Wofsy et al. (13)) and a clustered TCR distribution (this work) across the whole synapse. However, despite the relatively small numbers of engagements, the spatial and temporal proximity of TCR binding events probably has a major impact on signal transduction, perhaps due to spatiotemporal localization of signaling proteins in the cluster. In this work we looked only at physical stabilization of the TCR-pMHC bond by coreceptors and null pMHC. The presence of the coreceptor (and associated Lck) at the TCR during pMHC binding has been shown, experimentally and theoretically, to boost TCR signaling (31). Furthermore, it has been shown that stronger agonists are able to take better advantage of the pool of null or endogenous pMHC present on the APC (43). Further experimental and theoretical analysis will refine our understanding of the costs and benefits of TCR clustering on antigen detection and effector function.

Multiple cluster effects

We have calculated the degree of TCR engagement by a diffusing pMHC in a field of immobile TCR clusters and found that substantial engagement of clustered and nonclustered TCR is expected. However, experiments show no change in Zap-70 recruitment to nonclustered TCR once the TCR-pMHC interaction is blocked (21) suggesting that nonclustered TCR do not signal. Combined with our theoretical calculations these results further emphasize the importance of spatiotemporal localization of TCR engagements. Future particle tracking studies of labeled pMHC molecules (on a cell or supported bilayer) during T cell contact will inform us on the duration that they spend within clusters. Such studies will also resolve whether pMHC molecules move between clusters or remain in a single cluster during a journey to the cSMAC.

Importance of pMHC-TCR bond affinity

Fundamentally, T cell detection of pMHC rests on the TCR-pMHC interaction and is parameterized by just a few measured constants $-k_{on}$, k_{off}, and/or $K_D = k_{off}/k_{on}$. The importance of k_{off} has been emphasized in some studies (for instance, (16–18,45)) where an intermediate ''optimal'' lifetime is proposed to balance serial engagement with effective TCR signaling, suggesting that the K_D of the interaction is less important. On the other hand, Holler and Kranz (12) presents striking evidence for the importance of K_D. Here, we have found maximum values for K_D that allow effective pMHC transport, independent of the kinetic rate constants, and a potentially important role for factors strengthening the TCR-pMHC bond. The data presented in Tables 2 and 3 show no correlation between k_{off} and hits in the absence of coreceptors, but good correlation (for data from (43) and (12)) in the presence of coreceptors. More work is definitely needed to elucidate the importance of k_{off} versus K_D in T cell signaling.

Importance (or otherwise) of serial engagement of TCR

In this article, we have focused on calculating levels of serial engagement of TCR by pMHC. The importance of serial engagement to T cell activation, however, remains unclear. It has been shown that very few agonist pMHC are able to stimulate signaling downstream from the TCR within 5–10 s of contact (5,46). Furthermore, cytotoxic T cell killing can occur extremely rapidly, before the formation of the full immune synapse (47). On the other hand, sustained TCR signaling during a prolonged interaction (many hours) has been shown to be important for cytokine production and cellular proliferation (48). We suggest that there are different levels of TCR signaling, leading to various cellular responses, and that serial engagement of TCR by pMHC may be important for sustained signaling on the timescale of minutes to hours. Furthermore, the density of agonist pMHC for a particular T cell is probably lower in vivo than in the usual experimental situations and the TCR-pMHC bond may be weaker.

Understanding signal amplification by various mechanisms (coreceptor action, pMHC dimers and pseudodimers, serial engagement of TCR by pMHC, and serial encounters of T cells with APC) is a major theme in T cell activation research. Hopefully, our knowledge of the roles of these mechanisms will improve with new experimental and theoretical insights.

APPENDIX

In this section we use matched asymptotic analysis to solve for t_2 (Eq. 17b) in the limit that $b \to 0$. We begin by rescaling the equation for t_2 using $u = t_2/t^*$ and $\mathbf{x} = \mathbf{r}/R_s$. After some rearranging we obtain

$$\frac{\pi k_{\mathrm{off}} D_{\mathrm{P}} t^*}{\overline{k}_{\mathrm{on}} N_{\mathrm{T}}} \nabla^2 u = -\frac{R_{\mathrm{s}}^2}{b^2} I, \tag{21}$$

where we have used the fact that $T_{\mathrm{mc}} = N_{\mathrm{T}}/\pi b^2$. We identify the dimensionless quantity b/R_{s} with a small parameter $\epsilon = b/\mathrm{R_s}$ and define $t^* = \overline{k}_{\mathrm{on}} N_{\mathrm{T}}/\pi k_{\mathrm{off}} D_{\mathrm{P}}$. We obtain the following equation that we wish to solve in the limit $\epsilon \to 0$,

$$\nabla^2 u = -\frac{1}{\epsilon^2} \mathrm{I}_{\varepsilon}(\mathbf{x}; \mathbf{x}_1 \ldots \mathbf{x}_{\mathrm{N}}), \tag{22}$$

with $u(|\mathbf{x}| = 1) = 0$. The indicator function (Eq. 19) becomes

$$I_{\epsilon}(\mathbf{x}; \mathbf{x}_1, \ldots \mathbf{x}_{\mathrm{N}}) = \begin{cases} 1 & |\mathbf{x} - \mathbf{x}_{\mathrm{j}}| \le \epsilon \\ 0 & |\mathbf{x} - \mathbf{x}_{\mathrm{j}}| > \epsilon \end{cases}.$$

Inner solution

In the region near the j^{th} TCR microcluster we introduce the local space variable $\mathbf{y} = (\mathbf{x} - \mathbf{x}_{\mathrm{j}})/\epsilon$. Consequently we write $u^{\mathrm{in}}(\mathbf{y}) = u(\mathbf{x}_{\mathrm{j}} + \epsilon\, \mathbf{y})$ to obtain the governing equation near the j^{th} cluster,

$$\nabla_{\mathrm{y}}^2 u_{\mathrm{j}}^{\mathrm{in}} = \begin{cases} -1 & |\mathbf{y}| \le 1 \\ 0 & |\mathbf{y}| > 1 \end{cases}. \tag{23}$$

We expand the inner solution in powers of $v = -1/\log(\epsilon)$,

$$u_{\mathrm{j}}^{\mathrm{in}} = u_{\mathrm{j},-1} v^{-1} + u_{\mathrm{j},0} + \sum_{\mathrm{i}=1} v^{\mathrm{i}} u_{\mathrm{j,i}}, \tag{24}$$

where the i subscript indicates the order of the solution. Substituting Eq. 24 into Eq. 23 and matching orders of v we obtain

$$\begin{aligned} &v^{-1}; \nabla_{\mathrm{y}}^2 u_{\mathrm{j},-1} = 0 \\ &v^{0}; \nabla_{\mathrm{y}}^2 u_{\mathrm{j},0} = \begin{cases} -1 & |\mathbf{y}| \le 1 \\ 0 & |\mathbf{y}| > 1 \end{cases} \\ &v^{\mathrm{i}}; \nabla_{\mathrm{y}}^2 u_{\mathrm{j,i}} = 0, i \ge 1. \end{aligned} \tag{25}$$

The solution to the $i = 0$ equation is (up to an additive constant)

$$u_{\mathrm{j},0} = \begin{cases} -\frac{1}{2}\log|\mathbf{y}| & |\mathbf{y}| > 1 \\ \frac{1}{4}(1 - \mathbf{y}^2) & |\mathbf{y}| \le 1 \end{cases}.$$

The solutions to all other orders are $u_{\mathrm{j,i}} = c_1 \log|\,\mathbf{y}\,| + A_{\mathrm{j,i}}$ $(i \neq 0)$. We set $c_1 = 0$ to avoid blow-up. In summary, the solution to the inner problem around the j^{th} TCR microcluster is

$$u_{\mathrm{j}}^{\mathrm{in}} = A_{\mathrm{j},-1} v^{-1} + u_{\mathrm{j},0} + A_{\mathrm{j},0} + \sum_{\mathrm{i}=1} v^{\mathrm{i}} A_{\mathrm{j,i}}. \tag{26}$$

As $|\mathbf{y}| \to \infty$, the inner solution becomes

$$u_{\mathrm{j}}^{\mathrm{in}} = A_{\mathrm{j},-1} v^{-1} - \frac{1}{2}\log|\mathbf{x} - \mathbf{x}_{\mathrm{j}}| + \frac{1}{2}\log(\epsilon) + A_{\mathrm{j},0} + \sum_{\mathrm{i}=1} v^{\mathrm{i}} A_{\mathrm{j,i}}. \tag{27}$$

The unknown constants $A_{\mathrm{j,i}}$ will be determined by matching this exact inner solution with the outer solution.

Outer solution

The outer problem is

$$\nabla^2 u^{\mathrm{out}} = 0, \mathbf{x} \in \Omega \backslash \left\{ \sum_{\mathrm{i}=1} |\mathbf{x} - \mathbf{x}_{\mathrm{j}}| \le \epsilon \right\}, \tag{28}$$

with $u^{\mathrm{out}}(|\,\mathbf{x}\,| = 1) = 0$ and $u^{\mathrm{out}} \to -(1/2)\log(|\mathbf{x} - \mathbf{x}_{\mathrm{j}}|)$ as $\mathbf{x} \to \mathbf{x}_{\mathrm{j}}$. The related Green's function problem is

$$\nabla^2 \hat{G} = \delta(\mathbf{x} - \mathbf{x}_{\mathrm{k}}),\ \hat{G}(|\mathbf{x}| = 1) = 0. \tag{29}$$

Using the method of images the solution can be written as

$$\begin{aligned} &\hat{G}(\mathbf{x}, \mathbf{x}_{\mathrm{k}}) = G(\mathbf{x}, \mathbf{x}_{\mathrm{k}}) + R(\mathbf{x}, \mathbf{x}_{\mathrm{k}}), \quad \text{where} \\ &G(\mathbf{x}, \mathbf{x}_{\mathrm{k}}) = \frac{1}{2\pi}\log|\mathbf{x} - \mathbf{x}_{\mathrm{k}}| \quad \text{and} \\ &R(\mathbf{x}, \mathbf{x}_{\mathrm{k}}) = -\frac{1}{2\pi}\log\left[\frac{|\mathbf{x}|\mathbf{x}_{\mathrm{k}}|^2 - \mathbf{x}_{\mathrm{k}}|}{|\mathbf{x}_{\mathrm{k}}|}\right]. \end{aligned} \tag{30}$$

R is known as the regular part of the Green's function. We see that we obtain the required log dependence and consequently reformulate the outer problem as

$$\nabla^2 u^{\mathrm{out}} = -\pi \sum_{\mathrm{k}=1} \delta(\mathbf{x} - \mathbf{x}_{\mathrm{k}}),\ \mathbf{x} \in \Omega, \tag{31}$$

with $u^{\mathrm{out}}(|\,\mathbf{x}\,| = 1) = 0$. We write the solution in terms of the Green's function

$$u^{\mathrm{out}} = -\pi \sum_{\mathrm{k}=1} \hat{G}(\mathbf{x}, \mathbf{x}_{\mathrm{k}}). \tag{32}$$

As $\mathbf{x} \to \mathbf{x}_{\mathrm{j}}$, the solution becomes

$$u^{\mathrm{out}} = -\frac{1}{2}\log|\mathbf{x} - \mathbf{x}_{\mathrm{j}}| - \pi R(\mathbf{x}_{\mathrm{j}}, \mathbf{x}_{\mathrm{j}}) - \pi \sum_{\substack{\mathrm{k}=1 \\ \mathrm{k} \neq \mathrm{j}}} \hat{G}(\mathbf{x}_{\mathrm{j}}, \mathbf{x}_{\mathrm{k}}). \tag{33}$$

Matching condition

We can now match the inner expansion (Eq. 27) with the outer expansion (Eq. 33) to all orders of v. We obtain $A_{j,-1} = 1/2$; $A_{j,0} = -\pi R(\mathbf{x}_{\mathrm{j}}, \mathbf{x}_{\mathrm{j}}) - \pi \sum_{\substack{\mathrm{k}=1 \\ \mathrm{k} \neq \mathrm{j}}} \hat{G}(\mathbf{x}_{\mathrm{j}}, \mathbf{x}_{\mathrm{k}})$; and $A_{\mathrm{j,\,i}} = 0$ for $i \ge 1$. Therefore, the infinite expansion in the inner region reduces to just two terms.

Mean escape time

We compute the mean of u by averaging over the whole domain,

$$\langle u \rangle = \frac{1}{|\Omega|} \int \int_{\Omega} \left[(1 - I_{\epsilon}) u^{\mathrm{out}} + I_{\epsilon} \sum_{\mathrm{j}=1}^{\mathrm{N}} u_{\mathrm{j}}^{\mathrm{in}} \right] d\mathbf{x},$$

where the outer solution, Eq. 32, is valid outside clusters, and the inner solution, Eq. 26, is valid within clusters. Rearranging and computing the integral we obtain

$$\begin{aligned} \langle u \rangle = &\frac{1}{|\Omega|} \int \int_{\Omega} u^{\mathrm{out}} + \frac{1}{|\Omega|} \int \int_{\Omega} I_{\epsilon} \left[\sum_{\mathrm{j}=1}^{\mathrm{N}} u_{\mathrm{j}}^{\mathrm{in}} - u^{\mathrm{out}} \right] \\ &d\mathbf{x} = \frac{1}{4} \sum_{\mathrm{k}=1}^{\mathrm{N}} (1 - |\mathbf{x}_{\mathrm{k}}|^2) + \vartheta(\epsilon^2). \end{aligned} \tag{34}$$

We show how to explicitly compute the first integral below. The second integral is of order ϵ^2 because of the appearance of the indicator function, I_{ϵ}. Finally, we multiply $\langle u \rangle$ by t^* to obtain the unscaled quantity $\langle t_2 \rangle$. Assuming the initial position of the particle is within one of the N microclusters we may compute $\langle u \rangle$:

$$\langle u^{\text{in}}\rangle = \frac{1}{N\pi\epsilon^2}\int\int_{\Omega} I_\epsilon \sum_{\text{j}=1}^{\text{N}} u_{\text{j}}^{\text{in}}.$$

After computing the integral and unscaling the equation we obtain Eq. 20.

Mean escape time integral

In this section we evaluate the first integral in Eq. 34. After substituting the outer solution, Eq. 32, we obtain

$$\langle u\rangle = -\frac{\pi}{|\Omega|}\sum_{\text{k}=1}^{\text{N}}\int\int_{\Omega}\hat{G}(\mathbf{x},\mathbf{x}_{\text{k}}) = -\frac{\pi}{|\Omega|}\sum_{\text{k}=1}^{\text{N}}\left[L_{\text{k}}^1 + L_{\text{k}}^2\right], \quad (35)$$

where

$$L_{\text{k}}^1 = \frac{1}{2\pi}\int\int_{\Omega}\log|\mathbf{x}-\mathbf{x}_{\text{k}}|d\mathbf{x} \quad \text{and}$$
$$L_{\text{k}}^2 = -\frac{1}{2\pi}\int\int_{\Omega}\log\left||\mathbf{x}_{\text{k}}|\mathbf{x} - \frac{\mathbf{x}_{\text{k}}}{|\mathbf{x}_{\text{k}}|}\right|d\mathbf{x}. \quad (36)$$

We first calculate L_{k}^2. Without loss of generality we assume that $\mathbf{x}_{\text{k}}$ lies on the positive x axis and therefore we let $\mathbf{x} = re^{i\theta}\hat{\mathbf{r}}$ and $\mathbf{x}_{\text{k}} = \rho_{\text{k}}\hat{\mathbf{r}}$. With these we find

$$L_{\text{k}}^2 = -\frac{1}{2\pi}\int_0^{2\pi}d\theta\int_0^1 dr\log|\rho_{\text{k}}re^{i\theta}-1|. \quad (37)$$

Next we let $z = e^{i\theta}$ to obtain a computable contour integral,

$$L_{\text{k}}^2 = -\frac{1}{2\pi}\int_0^1 rdr\int_{|z|=1}dz\frac{-i\log|\rho_{\text{k}}rz-1|}{z}$$
$$= -\frac{1}{2\pi}\int_0^1 rdr(-i2\pi i\,\text{Res}(z=0))$$
$$= -\frac{1}{2\pi}\int_0^1 rdr(2\pi\log|-1|) = 0.$$

The only singularity for $|z|\le 1$ occurred where $z = 0$ and consequently we find $L_{\text{k}}^2 = 0$. To evaluate L_{k}^1, we make the same substitutions for $\mathbf{x}$ and $\mathbf{x}_{\text{k}}$ to obtain

$$L_{\text{k}}^1 = \frac{1}{2\pi}\int_0^{2\pi}d\theta\int_0^1 dr\log|re^{\text{i}\theta}-\rho_{\text{k}}|.$$

Here we cannot make the complex substitution directly since the log term will have a singularity within the contour integral. Instead, we rearrange the integrand to obtain

$$\log|re^{\text{i}\theta}-\rho_{\text{k}}| = \frac{1}{2}\log(r^2+\rho_{\text{k}}^2) + \frac{1}{2}\log(1-\mu\cos\theta), \quad (38)$$

where $\mu = 2r\rho_{\text{k}}/(r^2+\rho_{\text{k}}^2)$. Substituting and performing the integration over θ we obtain

$$L_{\text{k}}^1 = \frac{1}{2\pi}\int_0^1 rdr\left[\pi\log(r^2+\rho_{\text{k}}^2) + \pi\log\left(\frac{1+\sqrt{1-\mu^2}}{2}\right)\right],$$

where we have used the identity

$$\int_0^{2\pi}\log(1-\mu\cos\theta)d\theta = 2\pi\log\left(\frac{1+\sqrt{1-\mu^2}}{2}\right).$$

Next we note that

$$\frac{1+\sqrt{1-\mu^2}}{2} = \begin{cases}\dfrac{r^2}{r^2+\rho_{\text{k}}^2} & r>\rho_{\text{k}}\\ \dfrac{\rho_{\text{k}}^2}{r^2+\rho_{\text{k}}^2} & r<\rho_{\text{k}}\end{cases},$$

so we can establish

$$L_{\text{k}}^1 = \frac{1}{2\pi}\left[\pi\log(\rho_{\text{k}}^2)\int_0^{\rho_{\text{k}}}rdr + \pi\int_{\rho_{\text{k}}}^1 r\log(r^2)dr\right]$$
$$= \frac{1}{4}(\rho_{\text{k}}^2-1). \quad (39)$$

Finally, we combine the results for L_{k}^1 and L_{k}^2 to obtain

$$\langle u\rangle = -\frac{1}{4}\sum_{\text{k}=1}^{\text{N}}\left[|\mathbf{x}_{\text{k}}|^2-1\right], \quad (40)$$

where we have used $|\Omega| = \pi$ and $\rho_{\text{k}} = |\mathbf{x}_{\text{k}}|$.

We thank Raibatak Das, Michael Ward, Alan Lindsay, and especially Salvatore Valitutti and Rajat Varma for helpful discussions. We also thank Rajat Varma for supplying high-resolution images of TCR microclusters from Varma et al. (21).

This work was supported by National Sciences and Engineering Research Council (Canada) and Mathematics of Information Technology and Complex Systems Network of Centres of Excellence.

REFERENCES

1. Grakoui, A., S. K. Bromley, C. Sumen, M. M. Davis, A. S. Shaw, P. M. Allen, and M. L. Dustin. 1999. The immunological synapse: a molecular machine controlling T cell activation. *Science*. 285:221–227.
2. Cemerski, S., and A. Shaw. 2006. Immune synapses in T-cell activation. *Curr. Opin. Immunol.* 18:298–304.
3. Harding, C. V., and E. R. Unanue. 1990. Quantitation of antigen-presenting cell MHC class-II peptide complexes necessary for T-cell stimulation. *Nature*. 346:574–576.
4. Demotz, S., H. M. Grey, and A. Sette. 1990. The minimal number of class-II MHC antigen complexes needed for T-cell activation. *Science*. 249:1028–1030.
5. Irvine, D. J., M. A. Purbhoo, M. Krogsgaard, and M. M. Davis. 2002. Direct observation of ligand recognition by T cells. *Nature*. 419:845–849.
6. Davis, M. M., M. Krogsgaard, J. B. Huppa, C. Sumen, M. A. Purbhoo, D. J. Irvine, L. C. Wu, and L. Ehrlich. 2003. Dynamics of cell surface molecules during T cell recognition. *Annu. Rev. Biochem.* 72:717–742.
7. Valitutti, S., S. Muller, M. Cella, E. Padovan, and A. Lanzavecchia. 1995. Serial triggering of many T-cell receptors by a few peptide-MHC complexes. *Nature*. 375:148–151.
8. Itoh, Y., B. Hemmer, R. Martin, and R. N. Germain. 1999. Serial TCR engagement and down-modulation by peptide:MHC molecule ligands: relationship to the quality of individual TCR signaling events. *J. Immunol.* 162:2073–2080.
9. José, E. S., A. Borroto, F. Niedergang, A. Alcover, and B. Alarcón. 2000. Triggering the TCR complex cause the downregulation of non-engaged receptors by a signal transduction-dependent mechanism. *Immunity*. 12:161–170.
10. Sousa, J., and J. Carneiro. 2000. A mathematical analysis of TCR serial triggering and down-regulation. *Eur. J. Immunol.* 30:3219–3227.
11. Utzny, C., D. Coombs, S. Muller, and S. Valitutti. 2006. Analysis of peptide/MHC-induced TCR downregulation. *Cell Biochem. Biophys.* 46:101–111.
12. Holler, P. D., and D. M. Kranz. 2003. Quantitative analysis of the contribution of TCR/pepMHC affinity and CD8 to T cell activation. *Immunity*. 18:255–264.

13. Wofsy, C., D. Coombs, and B. Goldstein. 2001. Calculations show substantial serial engagement of T cell receptors. *Biophys. J.* 80:606–612.

14. McKeithan, K. 1995. Kinetic proofreading in T-cell receptor signal transduction. *Proc. Natl. Acad. Sci. USA.* 92:5042–5046.

15. Coombs, D., and B. Goldstein. 2005. T cell activation: Kinetic proofreading, serial engagement and cell adhesion. *J. Comput. Appl. Math.* 184:121–139.

16. Kalergis, A. M., N. Boucheron, M. A. Doucey, E. Palmieri, E. C. Goyarts, Z. Vegh, I. F. Luescher, and S. G. Nathenson. 2001. Efficient cell activation requires an optimal dwell-time of interaction between the TCR and the pMHC complex. *Nat. Immunol.* 2:229–234.

17. Coombs, D., A. M. Kalergis, S. G. Nathenson, C. Wofsy, and B. Goldstein. 2002. Activated TCR remain marked for internalization after dissociation from peptide-MHC. *Nat. Immunol.* 3:926–931.

18. Gonzalez, P. A., L. J. Carreno, D. Coombs, J. E. Mora, E. Palmieri, B. Goldstein, S. G. Nathenson, and A. M. Kalergis. 2005. T cell receptor binding kinetics required for T cell activation depend on the density of cognate ligand on the antigen-presenting cell. *Proc. Natl. Acad. Sci. USA.* 102:4824–4829.

19. Yokosuka, T., K. Sakata-Sogawa, W. Kobayashi, M. Hiroshima, A. Hashimoto-Tane, M. Tokunaga, and M. L. Dustin. 2005. Newly generated T cell receptor microclusters initiate and sustain T cell activation by recruitment of Zap70 and SLP-76. *Nat. Immunol.* 6:1253–1262.

20. Campi, G., R. Varma, and M. L. Dustin. 2005. Actin and agonist MHC-peptide complex-dependent T cell receptor microclusters as scaffolds for signaling. *J. Exp. Med.* 202:1031–1036.

21. Varma, R., G. Campi, T. Yokosuka, T. Saito, and M. L. Dustin. 2006. T cell receptor-proximal signals are sustained in peripheral microclusters and terminated in the central supramolecular activation cluster. *Immunity.* 25:117–127.

22. Garcia, K. C., C. A. Scott, A. Brunmark, F. R. Carbone, P. A. Peterson, I. A. Wilson, and L. Teyton. 1996. CD8 enhances formation of stable T-cell receptor MHC class I molecule complexes. *Nature.* 384:577–581.

23. Gao, G., J. Tormo, U. Gerth, J. Wyer, A. McMichael, D. Stuart, J. Bell, E. Jones, and B. Jakobsen. 1997. Crystal structure of the human CD8aa and HLA-A2. *Nature.* 387:630–634.

24. Janeway, C. A. 1992. The T cell receptor as a multicomponent signaling machine: CD4/CD8 coreceptors and CD45 in T cell activation. *Annu. Rev. Immunol.* 10:645–674.

25. Lee, K. H., A. R. Dinner, C. Tu, G. Campi, S. Raychaudhuri, R. Varma, T. N. Sims, W. R. Burack, H. Wu, J. Wang, O. Kanagawa, M. Markiewicz, P. M. Allen, M. L. Dustin, A. K. Chakraborty, and A. S. Shaw. 2003. The immunological synapse balances T cell receptor signaling and degradation. *Science.* 302:1218–1222.

26. Goldstein, B., R. Griego, and C. Wofsy. 1984. Diffusion-limited forward rate constants in two dimensions: application to the trapping of cell surface receptors by coated pits. *Biophys. J.* 46:573–583.

27. Dustin, M. L., L. M. Ferguson, P. Y. Chan, T. A. Springer, and D. E. Golan. 1996. Visualization of CD2 interaction with LFA-3 and determination of the two-dimensional dissociation constant for adhesion receptors in a contact area. *J. Cell Biol.* 132:465–474.

28. Shaw, A. S., and M. L. Dustin. 1997. Making the T cell receptor go the distance: a topological view of T cell activation. *Immunity.* 6:361–369.

29. Lee, K. H., A. D. Holdorf, M. L. Dustin, A. C. Chan, P. M. Allen, and A. S. Shaw. 2002. T cell receptor signaling precedes immunological synapse formation. *Science.* 295:1539–1542.

30. Wülfing, C., C. Sumen, M. D. Sjaastad, L. C. Wu, M. L. Dustin, and M. M. Davis. 2002. Costimulation and endogenous MHC ligands contribute to T cell recognition. *Nat. Immunol.* 3:42–47.

31. Li, Q. J., A. R. Dinner, S. Y. Qi, D. J. Irvine, J. B. Huppa, M. M. Davis, and A. K. Chakraborty. 2004. CD4 enhances T cell sensitivity to antigen by coordinating Lck accumulation at the immunological synapse. *Nat. Immunol.* 5:791–799.

32. Wyer, J. R., B. E. Willcox, G. F. Gao, U. C. Gerth, S. J. Davis, J. I. Bell, P. A. van der Merwe, and B. K. Jakobsen. 1999. T cell receptor and coreceptor CD8$\alpha\alpha$ bind peptide-MHC independently and with distinct kinetics. *Immunity.* 10:219–225.

33. Cho, B. K., K. C. Lian, P. Lee, A. Brunmark, C. McKinley, J. Z. Chen, D. M. Kranz, and H. N. Eisen. 2001. Differences in antigen recognition and cytolytic activity of $CD8^+$ and $CD8^-$ T cells that express the same antigen-specific receptor. *Proc. Natl. Acad. Sci. USA.* 98:1723–1727.

34. Reference deleted in proof.

35. Wulfing, C., I. Tskvitaria-Fuller, N. Burroughs, M. D. Sjaastad, J. Klem, and J. D. Schatzle. 2002. Interface accumulation of receptor/ligand couples in lymphocyte activation: methods, mechanisms, and significance. *Immunol. Rev.* 189:64–83.

36. Xiong, Y., P. Kern, H. Chang, and E. Reinherz. 2001. T cell receptor binding to a pMHCII ligand is kinetically distinct from and independent of CD4. *J. Biol. Chem.* 276:5659–5667.

37. van der Merwe, P. A., and S. J. Davis. 2003. Molecular interactions mediating T cell antigen recognition. *Annu. Rev. Immunol.* 21:659–684.

38. Thome, M., P. Duplay, M. Guttinger, and O. Acuto. 1995. Syk and ZAP-70 mediate recruitment of p56lck/CD4 to the activated T cell receptor/CD3/ζ complex. *J. Exp. Med.* 181:1997–2006.

39. Thome, M., V. Germain, J. P. DiSanto, and O. Acuto. 1996. The p56lck SH2 domain mediates recruitment of CD8/p56lck to the activated T cell receptor/CD3/zeta complex. *Eur. J. Immunol.* 26:2093–2100.

40. Schafer, P., and S. Pierce. 1994. Evidence for dimers of MHC class II molecules in B lymphocytes and their role in low affinity T cell responses. *Immunity.* 1:699–707.

41. Lindstedt, R., N. Monk, G. Lombardi, and R. Lechler. 2001. Amino acid substitutions in the putative MHC class II ''dimer of dimers'' interface inhibit CD4(+) T cell activation. *J. Immunol.* 166:800–808.

42. Cochran, J. R., T. O. Cameron, and L. J. Stern. 2000. The relationship of MHC-peptide binding and T cell activation probed using chemically defined MHC class II oligomers. *Immunity.* 12:241–250.

43. Krogsgaard, M., Q. J. Li, C. Sumen, J. B. Huppa, M. Huse, and M. M. Davis. 2005. Agonist/endogenous peptide-MHC heterodimers drive T cell activation and sensitivity. *Nature.* 434:238–243.

44. Vrljic, M., S. Y. Nishinura, S. Brasselet, W. E. Moerner, and H. M. McConnell. 2002. Translational diffusion of individual class II MHC membrane proteins in cells. *Biophys. J.* 83:2681–2692.

45. Lee, S.-J. E., Y. Hori, J. T. Groves, M. L. Dustin, and A. K. Chakraborty. 2002. Correlation of a dynamic model for immunological synapse formation with effector functions: two pathways to synapse formation. *Trends Immunol.* 23:492–499.

46. Li, Q. J., J. Chau, P. J. Ebert, G. Sylvester, H. Min, G. Liu, R. Braich, M. Manoharan, J. Soutschek, P. Skare, L. O. Klein, M. M. Davis, and C. Z. Chen. 2007. miR-181a is an intrinsic modulator of T cell sensitivity and selection. *Cell.* 129:147–161.

47. Purbhoo, M. A., D. J. Irvine, J. B. Huppa, and M. M. Davis. 2004. T cell killing does not require the formation of a stable mature immunological synapse. *Nat. Immunol.* 5:524–530.

48. Huppa, J. B., and M. M. Davis. 2003. T-cell-antigen recognition and the immunological synapse. *Nat. Rev. Immunol.* 3:973–983.

49. Saxton, M. J., and K. Jacobson. 1997. Single -particle tracking: applications to membrane dynamics. *Annu. Rev. Biophys. Biomol. Struct.* 26: 373–399.

50. Krogsgaard, M., N. Prado, E. J. Adams, X. L. He, D. C. Chow, D. B. Wilson, K. C. Garcia, and M. M. Davis. 2003. Evidence that structural rearrangements and/or flexibility during TCR binding can contribute to T cell activation. *Mol. Cell.* 12:1367–1378.

51. Garcia, K. C., C. G. Radu, J. Ho, R. J. Ober, and E. S. Ward. 2001. Kinetics and thermodynamics of T cell receptor-autoantigen interactions in murine experimental autoimmune encephalomyelitis. *Proc. Natl. Acad. Sci. USA.* 98:6818–6823.

52. Willcox, B. E., G. F. Gao, J. R. Wyer, J. E. Ladbury, J. I. Bell, B. K. Jakobsen, and P. A. van der Merwe. 1999. TCR binding to peptide-MHC stabilizes a flexible recognition interface. *Immunity.* 10:357–365.

53. Dushek, O., R. Das, and D. Coombs. Analysis of membrane-localized binding kinetics with FRAP. *Eur. Biophys J.* In press.